Research Article | Vol. 26, No. 2 | 22 Jan 2018 | OPTICS EXPRESS 870
Optics EXPRESS

Graded SiGe waveguides with broadband low-loss propagation in the mid infrared

J. M. RAMIREZ,[1,*] Q. LIU,[1] V. VAKARIN,[1] J. FRIGERIO,[2] A. BALLABIO,[2] X. LE ROUX,[1] D. BOUVILLE,[1] L. VIVIEN,[1] G. ISELLA,[2] AND D. MARRIS-MORINI[1]

[1]*Centre de Nanosciences et de Nanotechnologies, Université Paris Sud, CNRS, Université Paris Saclay, 91405 Orsay, France*
[2]*L-NESS, Dipartimento di Fisica, Politecnico di Milano, Polo di Como, Via Anzani 42, 22100 Como, Italy*
**joan-manel.ramirez@u-psud.fr*

Abstract: Mid-infrared (mid-IR) silicon photonics is expected to lead key advances in different areas including spectroscopy, remote sensing, nonlinear optics or free-space communications, among others. Still, the inherent limitations of the silicon-on-insulator (SOI) technology, namely the early mid-IR absorption of silicon oxide and silicon at λ~3.6 µm and at λ ~8.5 µm respectively, remain the main stumbling blocks that prevent this platform to fully exploit the mid-IR spectrum (λ ~2-20 µm). Here, we propose using a compact Ge-rich graded-index $Si_{1-x}Ge_x$ platform to overcome this constraint. A flat propagation loss characteristic as low as 2-3 dB/cm over a wavelength span from λ = 5.5 µm to 8.5 µm is demonstrated in Ge-rich $Si_{1-x}Ge_x$ waveguides of only 6 µm thick. The comparison of three different waveguides design with different vertical index profiles demonstrates the benefit of reducing the fraction of the guided mode that overlaps with the Si substrate to obtain such flat low loss behavior. Such Ge-rich $Si_{1-x}Ge_x$ platforms may open the route towards the implementation of mid-IR photonic integrated circuits with low-loss beyond the Si multi-phonon absorption band onset, hence truly exploiting the full Ge transparency window up to λ ~15 µm.

OCIS codes: (130.0130) Integrated optics; (230.0230) Optical devices; (230.7370) Waveguides.

References and links

1. L. Chrostowski and M. Hochberg, *Silicon Photonics Design: From Devices to Systems*, (Cambridge University, 2015).
2. R. Soref, "The past, present, and future of silicon photonics," IEEE J. Quantum Electron. **12**(6), 1678–1687 (2007).
3. D. J. Moss, R. Morandotti, A. L. Gaeta, and M. Lipson, "New CMOS-compatible platforms based on silicon nitride and Hydex for nonlinear optics," Nat. Photonics **7**(8), 597–607 (2013).
4. Y. A. Vlasov, "Silicon CMOS-integrated nano-photonics for computer and data communications beyond 100 G," IEEE Commun. Mag. **50**(2), S67 (2012).
5. R. Soref, "Mid-infrared photonics in silicon and germanium," Nat. Photonics **4**(8), 495–497 (2010).
6. T. Hu, B. Dong, X. Luo, T.-Y. Liow, J. Song, C. Lee, and G.-Q. Lo, "Silicon photonic platforms for mid-infrared applications," Photonics Res. **5**(5), 417 (2017).
7. V. Singh, P. T. Lin, N. Patel, H. Lin, L. Li, Y. Zou, F. Deng, C. Ni, J. Hu, J. Giammarco, A. P. Soliani, B. Zdyrko, I. Luzinov, S. Novak, J. Novak, P. Wachtel, S. Danto, J. D. Musgraves, K. Richardson, L. C. Kimerling, and A. M. Agarwal, "Mid-infrared materials and devices on a Si platform for optical sensing," Sci. Technol. Adv. Mater. **15**(1), 014603 (2014).
8. A. G. Griffith, R. K. Lau, J. Cardenas, Y. Okawachi, A. Mohanty, R. Fain, Y. H. Lee, M. Yu, C. T. Phare, C. B. Poitras, A. L. Gaeta, and M. Lipson, "Silicon-chip mid-infrared frequency comb generation," Nat. Commun. **6**, 6299 (2015).
9. C. Reimer, M. Nedeljkovic, D. J. M. Stothard, M. O. S. Esnault, C. Reardon, L. O'Faolain, M. Dunn, G. Z. Mashanovich, and T. F. Krauss, "Mid-infrared photonic crystal waveguides in silicon," Opt. Express **20**(28), 29361–29368 (2012).
10. M. Nedeljkovic, A. V. Velasco, A. Z. Khokhar, A. Delâge, P. Cheben, and G. Z. Mashanovich, "Mid-infrared silicon-on-insulator Fourier-transform spectrometer chip," IEEE Photonics Technol. Lett. **28**(4), 528–531 (2016).

#313442 https://doi.org/10.1364/OE.26.000870
Journal © 2018 Received 13 Nov 2017; revised 22 Dec 2017; accepted 22 Dec 2017; published 9 Jan 2018

Optics EXPRESS

11. B. Kuyken, X. Liu, R. M. Osgood, Jr., R. Baets, G. Roelkens, and W. M. J. Green, "Mid-Infrared to telecom-band supercontinuum generation in highly nonlinear silicon-on-insulator wire waveguides," Opt. Express **19**(21), 20172–20181 (2011).
12. S. A. Miller, M. Yu, X. Ji, A. G. Griffith, J. Cardenas, A. L. Gaeta, and M. Lipson, "Low-loss silicon platform for broadband mid-infrared photonics," Optica **4**(7), 707 (2017).
13. L. He, Y. Guo, Z. Han, K. Wada, L. C. Kimerling, J. Michel, A. M. Agarwal, G. Li, and L. Zhang, "Loss reduction of silicon-on-insulator waveguides for deep mid-infrared applications," Opt. Lett. **42**(17), 3454–3457 (2017).
14. T. Baehr-Jones, A. Spott, R. Ilic, A. Spott, B. Penkov, W. Asher, and M. Hochberg, "Silicon-on-sapphire integrated waveguides for the mid-infrared," Opt. Express **18**(12), 12127–12135 (2010).
15. Z. Cheng, X. Chen, C. Y. Wong, K. Xu, and H. K. Tsang, "Mid-infrared suspended membrane waveguide and ring resonator on silicon-on-insulator," IEEE Photonics J. **4**(5), 1510–1519 (2012).
16. J. S. Penades, A. Ortega-Moñux, M. Nedeljkovic, J. G. Wangüemert-Pérez, R. Halir, A. Z. Khokhar, C. Alonso-Ramos, Z. Qu, I. Molina-Fernández, P. Cheben, and G. Z. Mashanovich, "Suspended silicon mid-infrared waveguide devices with subwavelength grating metamaterial cladding," Opt. Express **24**(20), 22908–22916 (2016).
17. Y. C. Chang, V. Paeder, L. Hvozdara, J. M. Hartmann, and H. P. Herzig, "Low-loss germanium strip waveguides on silicon for the mid-infrared," Opt. Lett. **37**(14), 2883–2885 (2012).
18. M. Brun, P. Labeye, G. Grand, J. M. Hartmann, F. Boulila, M. Carras, and S. Nicoletti, "Low loss SiGe graded index waveguides for mid-IR applications," Opt. Express **22**(1), 508–518 (2014).
19. A. Malik, M. Muneeb, S. Pathak, Y. Shimura, J. Van Campenhout, R. Loo, and G. Roelkens, "Germanium-on-silicon mid-infrared arrayed waveguide grating multiplexers," IEEE Photonics Technol. Lett. **25**(18), 1805–1808 (2013).
20. B. Troia, J. S. Penades, A. Z. Khokhar, M. Nedeljkovic, C. Alonso-Ramos, V. M. N. Passaro, and G. Z. Mashanovich, "Germanium-on-silicon Vernier-effect photonic microcavities for the mid-infrared," Opt. Lett. **41**(3), 610–613 (2016).
21. A. Malik, M. Muneeb, Y. Shimura, J. Van Campenhout, and R. Loo, R., G. Roelkens, "Germanium-on-silicon mid-infrared waveguides and Mach-Zehnder interferometers," in *Photonics Conference (IPC)*, (2013), pp. 104–105.
22. M. Sinobad, P. Ma, B. Luther-Davies, D. Allioux, R. Orobtchouk, D. J. Moss, S. Madden, S. Boutami, J.-M. Fedeli, C. Monat, and C. Grillet, "Dispersion engineered air-clad SiGe waveguides with low propagation loss in the mid-infrared," in *CLEO Europe*, (2017), paper PD-2.5 WED.
23. M. Nedeljkovic, J. S. Penades, V. Mittal, G. S. Murugan, A. Z. Khokhar, C. LittleJohns, L. G. Carpenter, C. B. E. Gawith, J. S. Wilkinson, G. Mashanovich, "Germanium-on-silicon waveguides operating at mid-infrared wavelengths up to 8.5 µm," Opt. Express **25**(22), 27431 (2017).
24. J. Soler Penadés, A. Sánchez-Postigo, M. Nedeljkovic, A. Ortega-Moñux, J. G. Wangüemert-Pérez, Y. Xu, R. Halir, Z. Qu, A. Z. Khokhar, A. Osman, W. Cao, C. G. Littlejohns, P. Cheben, I. Molina-Fernández, and G. Z. Mashanovich, "Suspended silicon waveguides for long-wave infrared wavelengths," arXiv:1711.03468, (2017).
25. J. M. Ramirez, V. Vakarin, C. Gilles, J. Frigerio, A. Ballabio, P. Chaisakul, X. L. Roux, C. Alonso-Ramos, G. Maisons, L. Vivien, M. Carras, G. Isella, and D. Marris-Morini, "Low-loss Ge-rich Si0.2Ge0.8 waveguides for mid-infrared photonics," Opt. Lett. **42**(1), 105–108 (2017).
26. V. Vakarin, J. M. Ramírez, J. Frigerio, A. Ballabio, X. Le Roux, Q. Liu, D. Bouville, L. Vivien, G. Isella, and D. Marris-Morini, "Ultra-wideband Ge-rich silicon germanium integrated Mach-Zehnder interferometer for mid-infrared spectroscopy," Opt. Lett. **42**(17), 3482–3485 (2017).
27. J. M. Ramirez, V. Vakarin, J. Frigerio, P. Chaisakul, D. Chrastina, X. Le Roux, A. Ballabio, L. Vivien, G. Isella, and D. Marris-Morini, "Ge-rich graded-index Si1-xGex waveguides with broadband tight mode confinement and flat anomalous dispersion for nonlinear mid-infrared photonics," Opt. Express **25**(6), 6561–6567 (2017).
28. P. Chaisakul, D. Marris-Morini, J. Frigerio, D. Chrastina, M. S. Rouifed, S. Cecchi, P. Crozat, G. Isella, and L. Vivien, "Integrated germanium optical interconnects on silicon substrates," Nat. Photonics **8**(6), 482–488 (2014).
29. V. Raghunathan, R. Shori, O. M. Stafsudd, and B. Jalali, "Nonlinear absorption in silicon and the prospects of mid-infrared silicon Raman lasers," Phys. Status Solidi **203**(5), R38–R40 (2006).

1. Introduction

Research activities on silicon photonics have strongly increased over the last few years, giving birth to a dynamic technological network connecting research hubs, academics and new startup companies, all of them leveraging from the available mature industrial resources of the microelectronics industry. As a result, a large pool of outstanding works on novel silicon photonics assets has been reported so far, with especial attention to telecom applications working around of 1.31 µm and 1.55 µm [1–3]. In that regard, the possibility to link the long-haul optical communication fibers with high density data centers entirely driven by silicon photonics technology is conducting most of the efforts for this platform by now [4]. Lately however, silicon photonics has also been proposed as a compelling solution to address

Optics EXPRESS

several technical challenges in current biological and chemical sensing systems, taking advantage from the unique mid infrared (mid-IR) molecular absorption peaks of several relevant chemical compounds [5, 6]. Thus, scaling up silicon photonics to larger wavelengths in the mid-IR would lay the foundations of new integrated optical mid-IR lab-on-a-chip sensors with unprecedented sensitivity [7, 8]. A vast range of applications is foreseen, including real-time environmental monitoring of pollutants, food safety control or early medical diagnosis, among others. In pursuit of that goal, and in view of the good performance displayed in the near infrared range, the silicon-on-insulator platform has often been adopted as a natural choice to extend the wavelength of operation [9–11]. Nevertheless, the early mid-IR absorption onset of the buried oxide (BOX) at λ ~3.6 µm provides a strong inherent constraint that hinders the potentiality of this technology for mid-IR spectroscopy. In spite of that, various strategies have been proposed to overcome such limitation through waveguide design engineering to minimize the mode overlap with the BOX underneath [12, 13]. However no experimental demonstration beyond λ = 4 µm has been realized so far. Meanwhile, other Si-based platforms with extended spectral transparency in the mid-IR have been reported, such as Si-on-sapphire [14], suspended membranes schemes [15, 16], Ge-on-Si platforms [17] or the use of $Si_{1-x}Ge_x$ alloys on Si substrates [18]. Approaches using Ge are particularly interesting due to its large transparency window up to a wavelength of ~15 µm, hence broadening the range of substances that could potentially be analyzed. Still, most of the current demonstrations of Ge-based mid-IR devices reported in the literature are confined to relatively narrow operation bandwidths, hence squandering the potential of the platform [19–22]. Noticeably, recent work on Ge-on-Si waveguides reported the propagation loss characteristic from 7.5 to 8.5 µm wavelength, with a minimum value of 2.5 dB/cm at λ ~7.5 µm. However losses rapidly increased for longer wavelengths up to 20 dB/cm [23]. Alternatively, suspended Si waveguides have shown low-loss propagation up to 7.7 µm [24]. On the other hand, we have recently proposed Ge-rich $Si_{1-x}Ge_x$ alloys on graded $Si_{1-x}Ge_x$ layers as an alternative approach for mid-IR integrated photonics. Propagation losses between 1.5 and 2 dB/cm have been obtained at λ ~4.6 µm [25], while broadband Mach–Zehnder interferometers have been demonstrated, working in both quasi-TE and TM polarizations [26]. Interestingly, these structures also allow to fine tune the refractive index profile, permitting an efficient tailoring of the waveguide properties such as mode confinement and dispersion. An optimal design was investigated and a graded 6 µm-thick $Si_{1-x}Ge_x$ stack was defined as an attractive platform to develop mid-IR nonlinear approaches requiring broadband dispersion engineering [27]. One of the relevant features of such Ge-rich $Si_{1-x}Ge_x$ waveguides is their expected wide transparency window, which could potentially extend up to λ = 15 µm, as the refractive index gradient allows to push the optical mode far from the Si substrate where absorption begins to be prohibitive beyond λ ~8.5 µm [5].

In this work we demonstrate a highly compact 6 µm thick Ge-rich graded-index $Si_{1-x}Ge_x$ platform with low-loss from 5.5 to 8.5 µm wavelength, only limited by the experimental set-up. In addition, we provide solid experimental evidences that support the importance of reducing the mode overlap with the Si substrate to obtain this low-loss mid-IR integrated waveguide. These new platforms may pose the foundations for a new generation of mid-IR integrated devices with unprecedented operation bandwidths.

2. Experiments and methods

Three different Ge-rich graded-index epilayers have been deposited over commercial Si (001) substrates by means of Low Energy Plasma Enhanced Chemical Vapor Deposition (LEPECVD) at a rate of 5-10 nm/s. Different Ge concentration profiles have been defined along the growth direction. Figure 1 provides a cross-section view of each epilayer ((a), (b) and (c)) together with its refractive index profile ((d), (e) and (f)). Waveguides with a width of W = 4 µm and an etching depth of ED = 4 µm have been defined. The simulated fundamental TE mode at λ = 7.5 µm is also shown for comparison. As seen in Fig. 1, epilayer

Optics EXPRESS

(a) (named Ge-rich + buffer) is composed by a graded buffer layer 11 μm thick with a linear increase of the Ge concentration up to a value of 79%, with a 2 μm thick Ge-rich $Si_{0.2}Ge_{0.8}$ guiding layer deposited on top (total thickness of t = 13 μm). Such configuration provides a small refractive index step at the guiding layer-graded buffer interface (see Fig. 1(d)) that has proven to be very useful to guide the optical mode while providing low-loss propagation at near infrared wavelengths [28]. Benchmarking results were also obtained in the mid-IR with this platform, demonstrating ultra-wideband Mach-Zehnder interferometers operating over a wavelength range from λ = 5.5 μm to 8.5 μm [25, 26].

Likewise, a graded buffer layer from pure Si to pure Ge (100%) was used to grow the second guiding platform under study (epilayer (b) in Fig. 1, named graded buffer). This time the mode directly propagates into the graded buffer, with no constant composition layer on top. Also, in order to improve the vertical confinement of the guided mode, a steeper Ge content increase was used as the total graded buffer thickness was t = 6 μm and the refractive index profile varied from n ~3.48 (Si) to n ~4.1 (Ge) (see Fig. 1(e)). This approach yields higher optical confinement by taking advantage of a steeper vertical refractive index profile compared to platform (a), at the expense of a potentially higher losses due to larger overlap between the guided mode and the Si substrate (further discussion is provided later on). In addition, this platform with the current waveguide design (i.e W = ED = 4 μm) shows interesting features that could potentially be exploited for $\chi^{(3)}$ nonlinear phenomena, such as a good overlap between the propagating mode and the Ge-rich area and a flat anomalous dispersion over a broadband wavelength range from λ = 3 μm to 8 μm [27].

Finally, we have devised a third Ge-based platform (epilayer (c)) comprising two different vertical Ge profiles for a total thickness of 4 μm to provide an even more compact stack while maintaining a good mode confinement (named as double graded buffer). In this case, a first graded-index layer 3 μm thick has been grown with an increasing Ge concentration in the growth direction from pure Si up to 50% of Ge ($Si_{0.5}Ge_{0.5}$). Then, a second graded-index buffer, 1 μm thick, is deposited on top, with a starting Ge concentration of 50% up to pure Ge (100%). Thus, the latter approach stands as the most compact among the three platforms here presented (only 4 μm thick in total), with the steepest refractive index profile which would potentially lead to stronger mode confinement over a large bandwidth (as seen in Fig. 1(f)).

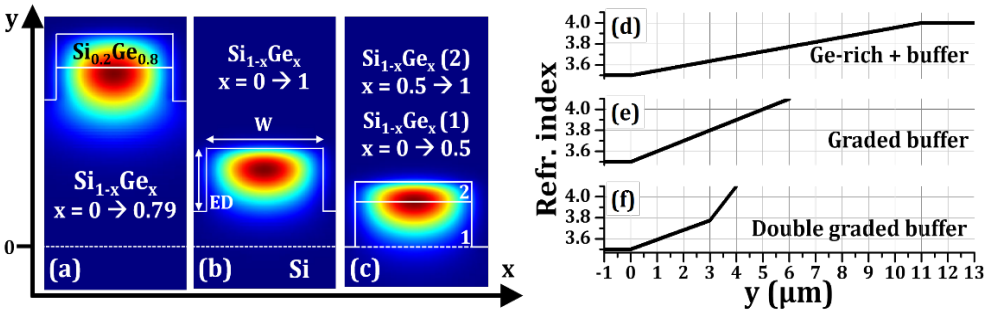

Fig. 1. Simulated fundamental TE mode at λ = 7.5 μm for the three studied waveguide approaches (panels (a), (b), (c)) with their corresponding refractive index profiles along the vertical direction (figures (d), (e), (f)). The x- and y-axis represent the simulation cross-section plane, with the y-axis origin marked by a horizontal dotted line.

The propagation loss of each platform was inspected by fabricating a set of spiral waveguides with different lengths (0.6 cm/4.2 cm/6.1 cm/8.3 cm and 10.4 cm) to allow for non-destructive transmission measurements using the cut-back method (see Fig. 2(a)). A minimum bend radius of 600 μm was designed in each spiral to discard any source of radiative loss due to bending, especially for the longest wavelengths. Similarly, adjacent concentric rings have been spaced by 50 μm to avoid cross-talk effects (see Fig. 2(b)). Adiabatic tapers 50 μm wide and 2 mm long have also been designed to minimize coupling

Optics EXPRESS

losses between the free-space laser beam and the spiral waveguides. Waveguide spirals were patterned by optical lithography using a DUV photoresist. Then, Inductively Coupled Plasma (ICP) etching was performed to define the waveguides, followed by a wet processing using hydrogen peroxide (H_2O_2) to smooth the sidewall roughness. Waveguides facets were defined by mechanical dicing, obtaining a smooth facet upon which reproducible coupling conditions have been obtained.

Measurements were performed using an ad hoc free-space mid-IR setup. This configuration allows controlling precisely the injected polarization, contrarily to currently available fiber-based mid-IR approaches. The set-up was placed inside an isolation box and equipped with a dry air filling system, to reduce the impact of the multiple atmospheric absorption peaks that arise within this wavelength range. Transmission measurements were performed using a mid-IR tunable external cavity quantum cascade laser (MIRCAT) operating in pulsed regime with a duty cycle of 5% and a repetition rate of 100 kHz. The laser provides an attainable wavelength range from λ = 5.5 µm to λ = 8.5 µm, with a maximum peak power of 300 mW (at λ = 6.5 µm) and a wavelength accuracy lower than 1 cm^{-1}. The wavelength scan has been performed in steps of 4 nm per second. Since the laser emission is TM polarized, a broadband mid-IR polarization rotator was placed at the laser output to rotate the laser beam polarization at will. Input/output chip butt-coupling was carried out by means of aspheric ZnSe lenses. The collected signal was directed towards a polarization filter to discard any polarization rotation throughout the spiral waveguides, and finally sent to either an MCT detector or a mid-IR camera by means of a movable mid-IR mirror. Observing the mode profile allows us to ensure that light is coupled on the fundamental mode of the waveguide. Figure 2(c) shows a representative example of a far-field optical mode at the spiral waveguide output recorded by the mid-IR camera. Finally, a lock-in amplifier was used to synchronize the laser with the signal from the MCT detector.

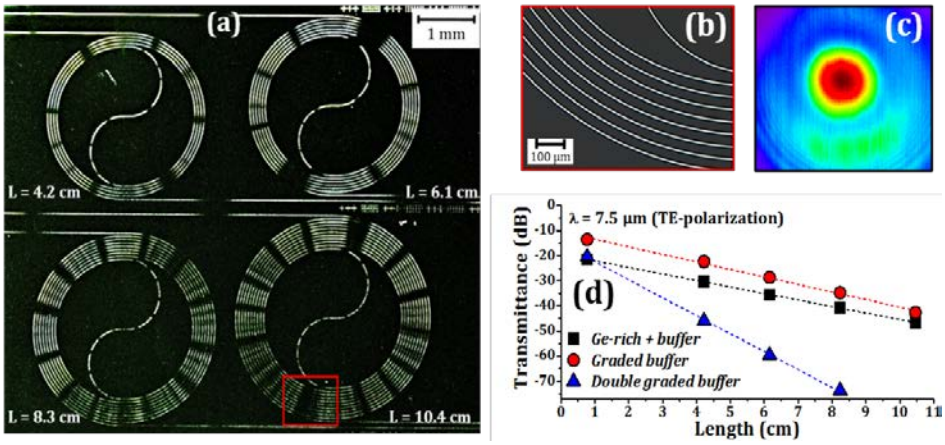

Fig. 2. (a) Top view of the fabricated $Si_{1-x}Ge_x$ spiral waveguides. (b) Magnified region of a single spiral waveguide corresponding to the red square area depicted in (a). (c) Typical far-field optical mode recorded at the waveguide output facet by the mid-IR camera. (d) Output signal transmittance of the quasi-TE propagating polarization as a function of the spiral waveguide length for a wavelength of λ = 7.5 µm. Dashed colored lines are linear fits of the data.

3. Results

Figure 2(d) shows a representative cut-back measurement of the three different platforms performed at λ = 7.5 µm (quasi-TE polarization) in which the output transmittance of each spiral waveguide has been plotted as a function of its total length. As can be observed, the measured transmittance linearly decreases with the spiral waveguide length, whose slope can be directly correlated with the propagation loss in each platform. As seen, whereas the two

Optics EXPRESS

first graded-index platforms show a rather similar propagation loss at λ = 7.5 µm, a remarkably higher value is found in the double graded buffer. Thus, performing the same fitting for each wavelength over the studied range (from λ = 5.5 µm to 8.5 µm in steps of 4 nm) allows obtaining the propagation loss spectral characteristic (see Fig. 3) of the three studied platforms for both input polarizations (black lines corresponding to quasi-TE polarization and red lines to quasi-TM polarization).

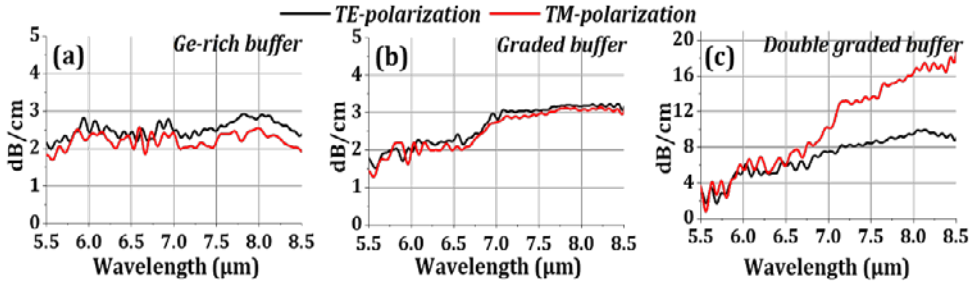

Fig. 3. Propagation loss measured over a wavelength span from λ = 5.5 µm to λ = 8.5 µm for the three studied platforms.

As seen, designs showing thicker waveguides cores (the Ge-rich + buffer with t = 13 µm, and the Graded buffer with t = 6 µm) present broadband low-loss propagation with values of 2-3 dB/cm in both polarizations and a nearly negligible wavelength dependency. Importantly, the measured propagation loss remains consistently low for wavelengths up to the longest available wavelength at λ = 8.5 µm. On the contrary, the propagation loss characteristic of the most compact approach (Fig. 3(c)) shows a consistent increase as a function of the operating wavelength with notable different values depending on the transmitted polarization. At λ = 5.5 µm, the propagation loss of both polarizations departs from a similar value than the ones measured for the two other platforms, i.e. 2-3 dB/cm. However, as the operating wavelength is increased, the propagation loss monotonically increases accordingly, reaching values of ~10 dB/cm for the quasi-TE mode and up to ~18 dB/cm for the quasi-TM polarization for the longest measured wavelength, at λ = 8.5 µm. Noteworthy, the propagation loss difference among transmitted polarizations becomes more evident at longer wavelengths beyond λ ~7 µm, with substantially higher values for the quasi-TM polarization. Such difference is unlikely to be caused by an enhanced scattering loss condition between one of the propagating modes and the waveguide sidewall roughness, as if that were the case, higher propagation losses would be expected for the quasi-TE mode since this polarization is known to be more sensitive to sidewall imperfections. Similarly, free carrier absorption which is expected to be greater in Ge than in Si and that increases strongly with wavelength cannot be the origin for the high losses in the double graded buffer waveguide as it would affect also the two other platforms. To explain the polarization-selective loss characteristic of the double graded buffer waveguide at long wavelengths, a modal analysis using the finite-element-method (FEM) has been performed in the double graded buffer platform (t = 4 µm) for a wavelength span from λ = 5.5 µm to 8.5 µm. For the sake of comparison, a similar study has also been conducted for the graded buffer approach (t = 6 µm).

Optics EXPRESS

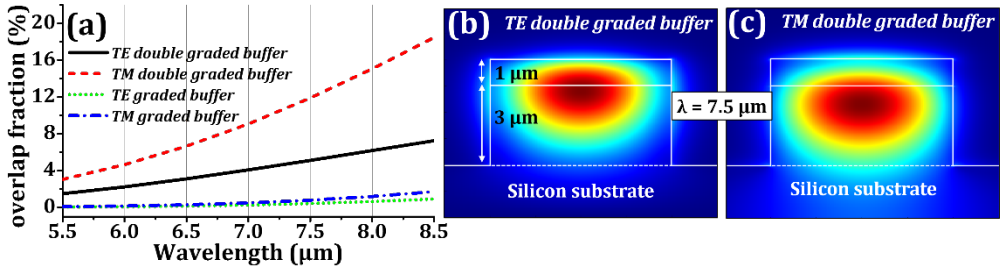

Fig. 4. (a) Evolution of the optical mode overlap with the Si substrate as a function of the operating wavelength for the double graded-index platform 4 μm thick (black straight line for quasi-TE and red dashed line for quasi-TM) and the graded-index layer 6 μm thick (green dotted line for quasi-TE and blue dashed-dotted line for quasi-TM). FEM simulations of the optical mode confinement in the double graded buffer platform are shown in (b) and (c) for the quasi-TE and quasi-TM polarizations, respectively. Simulations were conducted at a wavelength of λ = 7.5 μm.

Figure 4(a) reports the fraction of the guided optical mode that overlaps with the Si substrate. As can be observed, the graded buffer platform presents a very small mode overlap with the Si substrate, with a fraction below 1% up to a wavelength of λ ~7.5 μm regardless of the polarization, then showing a mild increase to a final value of ~1% (quasi-TE) and ~2% (quasi-TM) for λ ~8.5 μm. On the contrary, remarkable mode overlap with the Si substrate was obtained in the double graded buffer platform, especially for the quasi-TM polarization, which provides a sequential increase of the overlap fraction from 3% (at λ = 5.5 μm) up to 18% (at λ = 8.5 μm). In contrast, the quasi-TE polarization departs from a moderate value of 1.5% (at λ = 5.5 μm) up to a 7% (at λ = 8.5 μm) evidencing significant differences between each polarization. As a representative example, Fig. 4(b) and 4(c) compare the simulated quasi-TE and quasi-TM fundamental optical modes for λ = 7.5 μm in the double graded buffer platform, where it can be noticed at a first glance that the quasi-TE optical mode is confined at a substantially higher position in the waveguide compared to the quasi-TM optical mode.

Thus, since these results follow a similar trend than the measured propagation loss characteristic of the double graded buffer observed at Fig. 3(c), we could conclude that the wavelength-dependent propagation loss increase can be due to the partial overlap between the optical mode with the Si substrate, which may affect propagation losses through mechanisms such as Si multi-phonon absorption in the mid-IR range, whose onset is located around of λ ~7 μm [29]. Nevertheless, it should be noted that although good agreement between the spectral shape of the measured propagation loss characteristic and FEM simulations was obtained, the reported increase of optical loss in the double graded buffer platform is much higher than the one that could be expected from multi-phonon absorption in Si, according to available data (see ref. 29). Thus, at the current stage, the conclusion is that even if the exact origin of the propagation losses is not fully understood, the most compact platform (total thickness of 4 μm) may be strongly affected by the interaction of the optical mode with the Si substrate.

4. Conclusions

In summary, we demonstrated the potential of Ge-rich graded-index $Si_{1-x}Ge_x$ layers to be used as versatile and compact low-loss mid-IR photonic integrated platforms on Si substrates with an unprecedented transparency bandwidth. To this purpose, we exploited the vertical refractive index variation in compact graded $Si_{1-x}Ge_x$ buffer layers as an additional parameter to engineer broadband low-loss waveguides with the optical mode confined in the uppermost part of the structure, far away from the Si substrate interface. A compact graded-index waveguide approach has been conceived, yielding high optical mode confinement by means of a thorough design engineering of the vertical Ge concentration profile. Broadband low-loss

Optics EXPRESS

propagation of 2-3 dB/cm over a wavelength span from 5.5 µm to 8.5 µm is observed, being such extreme values only limited by the available wavelength scan of the experimental setup. Moreover, experimental evidences of the key role of the optical mode overlap with the Si substrate on the waveguide propagation loss are provided using an ultra-compact waveguide design with a total thickness of only 4 µm. These results provide the first experimental demonstration of the effect of the refractive index gradient to push the mode far away from the Si substrate to achieve low propagation loss over a wide spectral band, hence paving the road for future demonstration of passive and active devices for spectroscopy and telecom applications up to 15 µm.

Funding

European Research Council (ERC) under the European Union's Horizon 2020 research and innovation program (N°639107-INsPIRE).).

Acknowledgments

The fabrication of the device was performed at the Plateforme de Micro-Nano-Technologie/C2N, which is partially funded by the "Conseil Général de l'Essonne". This work was partly supported by the French RENATECH network. The Authors also thank Michele Ortolani for his advice in setting-up the mid-IR optical measurement apparatus.